DOI 10.1007/s10946-024-10217-2
Journal of Russian Laser Research, Volume 45, Number 3, May, 2024

TUNABLE ORTHOGONAL POLARIZED DUAL-WAVELENGTH Pr^{3+}: $LiGdF_4$ LASERS IN THE VISIBLE RANGE

Baozeng Li,[1*] Yongliang Li,[2] Zonghua Hu,[3] and Zhenhua Du[4]

[1] *School of Physics, Changchun University of Science and Technology Changchun 130022, China*

[2] *School of Optoelectronics Engineering, Changchun University of Science and Technology Changchun 130022, Jilin, China*

[3] *School of Physics and Technology, Minzu Normal University of Xingyi Xingyi 562400, China*

[4] *School of Physical Science and Technology, Bohai University Jinzhou 121013, China*

*Corresponding author e-mail: libaozeng1979@163.com

Abstract

We experimentally demonstrate for the first time a tunable orthogonal polarized Pr^{3+}: $LiGdF_4$ dual-wavelength laser. We calculate the conditions for balancing the gain and loss of the orthogonal polarization dual-wavelength with the rotation angles, the Lyot filter, and the incident angle on the uncoated glass. By adjusting the rotation angles, the Lyot filter, and the incident angle on the uncoated glass, the continuous-wave (CW) orthogonal polarized dual-wavelength lasers operating at 519.6 and 522.8 nm, 604.5 and 607.2 nm, and 719.2 and 721.5 nm are obtained.

Keywords: solid-state laser, tunable, visible dual-wavelength, Pr^{3+}: $LiGdF_4$.

1. Introduction

Multi-wavelength operation can produce wavelength beating and extends the capabilities of a laser source by multi-wavelength engineered emission, in which there are minimum two independent obtainable wavelengths. Two independent engineered wavelengths produced by the same laser have been used in optical coherence tomography, optical shop testing, atom interferometry, spectroscopy and even to detect parasites in water [1–6]. Dual-wavelength emission has been obtained using diode lasers, fiber lasers, and dye lasers [7–12]. Sources with emission in two wavelengths, using Titanium-sapphire lasers have also been explored with coupled cavities, double-prism dispersion cavities, acousto-optic tunable filters, as well as with two independent seed injection lasers [13–19]. So far, dual-wavelength lasers for different transitions of Nd^{3+} have been reported for some crystals, such as Nd:YAG, Nd:YVO_4, Nd:$GdVO_4$, Nd:$LuVO_4$, Nd:$YAlO_3$, Nd:GSAG, Nd:LSO, Nd:LYSO, Nd:SYSO, and Nd:YAB [20–29]. However, very few research works on dual-wavelength Nd^{3+}-doped lasers in the visible spectral region have been reported [30–32]. The main reason is that radiation in the visible spectral region cannot be generated because of the absence of efficient fundamental lasers. In the recent years, interest is growing for the development of all-solid state laser sources emitting in the visible region of the electromagnetic spectrum. One of the most promising candidates within the Rare Earth ions is trivalent Praseodymium (Pr^{3+}), offering

Manuscript submitted by the authors in English on April 25, 2024.

several transitions with high cross sections in the visible spectral regions. During the past decade, efficient cw single wavelength laser for different transitions of Pr^{3+} have been demonstrated for some crystals, such as $Pr^{3+}:LiYF_4$ [33–38], $Pr^{3+}:LiLuF_4$ [39–42], $Pr^{3+}:KY_3F_{10}$ [43–46], $Pr^{3+}:LiGdF_4$ [47], and $Pr:BaY_2F_8$ [48]. J. Xia et al. realized a visible dual-wavelength generation in Pr^{3+}-doped lasers for the first time [49]. J. Bai et al. obtained a red and green dual-wavelength $Pr:LiGdF_4$ laser with a single birefringent filter [50]. J. He et al. reported a tunable dual-wavelength laser operation of $Pr^{3+}:LiYF_4$, which was the first work of realizing dual-wavelength Pr^{3+}-doped laser operation in the infrared spectral range [51]. To the best of our knowledge, no research about tunable dual-wavelength Pr^{3+}-doped lasers in the visible spectral regions has been reported. In this paper, we present our recent results of exploring a tunable CW dual-wavelength laser operation of $Pr^{3+}:LiGdF_4$. This is the first work of realizing simultaneous dual-wavelength Pr^{3+}-doped laser operation in the visible spectral regions. Dual-wavelength laser in the visible spectral range can find wide applications in many fields, such as display technology, spectral analysis, medical applications, etc.

In Fig. 1, we show the polarized emission spectra of $Pr^{3+}:LiGdF_4$ crystal at room temperature. The highest emission cross sections of $Pr^{3+}:LiGdF_4$ crystal are present in the green (522.8 nm), orange (607.2 nm), and red (640.2 and 721.5 nm) spectral ranges in π-polarization ($E\|c$) [47]. In addition, there are some central emission wavelengths; for example, 519.6, 604.5, and 719.2 nm in σ-polarization ($E\perp c$). Therefore, $Pr^{3+}:LiGdF_4$ crystal is the promising material for use in orthogonal polarized dual-wavelength lasers.

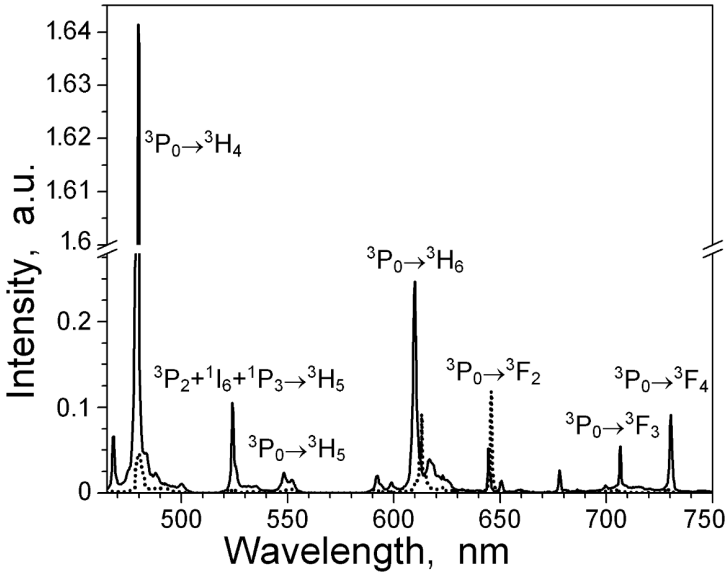

Fig. 1. Polarized $E\|c$ (the solid curve) and $E\perp c$ (the dotted curve) emission spectra of $Pr^{3+}:LiGdF_4$ crystal at λ_p = 442 nm [47].

2. Experiment and Analysis

The experimental setup used is shown in Fig. 2.

A 3 mm long sample with a dopand concentration of 1.0 at.% Pr^{3+} in the crystal is used in the laser experiment, resulting in an absorption coefficient of about 7.6 cm^{-1} [47]. The $Pr^{3+}:LiGdF_4$ laser crystal is pumped by two diode lasers emitting at 442 nm with a maximum output power of 2 W each. Beam collimation and shaping of the diode laser radiation is accomplished, using a spherical lens with a focal length of 20 mm as well as an anamorphic cylindrical lens pair. The lenses L1 and L2 of 40 mm focal length are used to focus the pump beams into the laser crystal. The beam waist diameter inside the crystal is approximately 100 μm. The pumping side of the $Pr^{3+}:LiGdF_4$ crystal (S1) is used as an input coupler, which is antireflection (AR) coated at 442 nm and high reflectivity (HR) coated at 510–730 nm. The opposite side is AR coated at 520–730 nm. The plane-folding input coupler (M1) is HR coated at 510–730 nm and AR coated at 442 nm. The $Pr^{3+}:LiGdF_4$ crystal wrapped with Indium foil and mounted at a TEC (thermal electronic cooled) Copper block, and the temperature is maintained at 20° C. The concave mirror (M2) with a radius of curvature −50 mm is used as the output coupler, with a transmission of 5.0% near 510–730 nm. An uncoated glass etalon with a thickness of

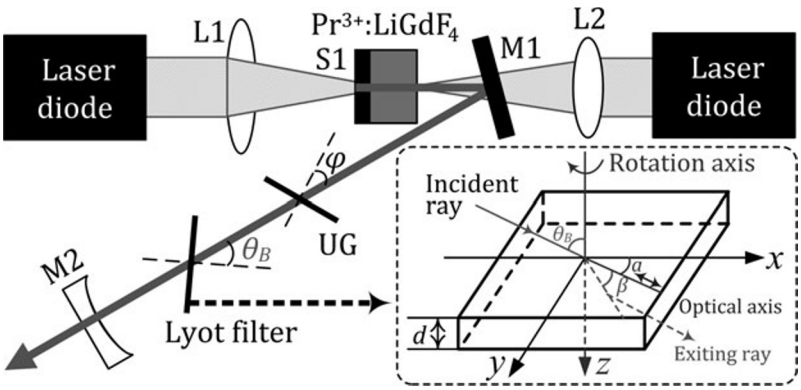

Fig. 2. The experimental setup for the tunable orthogonal polarized Pr^{3+}: $LiGdF_4$ dual-wavelength lasers in the visible range. Here, coupling lenses (L1 and L2), side of the Pr^{3+}: $LiGdF_4$ crystal (S1), input coupler (M1), output coupler (M2), and uncoated glass (UG).

0.2 mm is used to nearly fit the wavelength separation between two fluorescence peak positions of π and σ-polarizations near 510–730 nm in Pr^{3+}: $LiGdF_4$ crystal. The Lyot filter with a thickness of 1.5 mm is used as a tuning device. The Lyot filter is tilted so, that the angle of incidence is the Brewster angle θ_B.

Usually, simultaneous dual-wavelength operation with the same laser medium in the same cavity is rather difficult, because of strong gain competition between the two wavelengths. For achieving the dual-wavelength operation, an uncoated glass etalon is inserted in the laser cavity. In our experiment, the π-polarization of the Pr^{3+}: $LiGdF_4$ crystal is set to be placed in the parallel direction, and the angle of inclination of the glass plane is relative to the optical axis of the resonator, in which the plane of incidence is in the horizontal direction. As a result, the π and σ-polarized waves are perpendicularly and parallel to the plane of incidence, corresponding to the S and P waves, respectively. The inclined angle of the etalon is equal to the incident angle of light. The losses caused by the Fresnel reflection for the π and σ-polarized waves can be given by [52]

$$L_{g\pi} = \left(\frac{\cos\phi_i - n_g\cos\phi_t}{\cos\phi_i - n_g\cos\phi_t}\right)^2 + \left[1 - \left(\frac{\cos\phi_i - n_g\cos\phi_t}{\cos\phi_i - n_g\cos\phi_t}\right)^2\right] \cdot \left(\frac{n_g\cos\phi_t - \cos\phi_i}{n_g\cos\phi_t - \cos\phi_i}\right)^2, \quad (1)$$

$$L_{g\sigma} = \left(\frac{n_g\cos\phi_i - \cos\phi_t}{n_g\cos\phi_i - \cos\phi_t}\right)^2 + \left[1 - \left(\frac{n_g\cos\phi_i - \cos\phi_t}{n_g\cos\phi_i - \cos\phi_t}\right)^2\right] \cdot \left(\frac{\cos\phi_t - n_g\cos\phi_i}{\cos\phi_t - n_g\cos\phi_i}\right)^2, \quad (2)$$

where θ_i is the inclined angle of the glass plane (equal to the incident angle of light), θ_t is the refraction angle of light, $n_g = 1.5$ is the refractive index of the glass, and $\sin\phi_i = n_g \sin\phi_t$. In Fig. 3, one can see the overlapping curves for the losses $L_{g\pi}$ and $L_{g\sigma}$ at the small incident angle, and then they gradually separate.

For tuning the dual-wavelength of orthogonal polarization, a Lyot filter is inserted in the laser cavity. An incident ray lies in the xz plane and enters a uniaxial crystal plate at an incidence angle θ_B. The thickness of the plate is d, and its optical axis is parallel to the surface. The azimuth angle (or the rotation angle) α is the angle between the optical axis and x axis. The Lyot filter is rotated to have an azimuth angle α. The round-trip Jones matrix for the linear cavity is

$$M = \begin{pmatrix} 1 & 0 \\ 0 & q' \end{pmatrix}^2 \left[\begin{pmatrix} 1 & 0 \\ 0 & q \end{pmatrix} \begin{pmatrix} \sin\alpha & \cos\alpha \\ -\cos\alpha & \sin\alpha \end{pmatrix} \begin{pmatrix} 1 & 0 \\ 0 & e^{i\delta} \end{pmatrix} \begin{pmatrix} \sin\alpha & -\cos\alpha \\ \cos\alpha & \sin\alpha \end{pmatrix} \begin{pmatrix} 1 & 0 \\ 0 & q \end{pmatrix}\right]^2, \quad (3)$$

where $q = 2n/(1+n^2)$, n is the refractive index of the Lyot filter, $q = 0.916$, $q' = 0.876$, $\delta = \pi(n_o -$

$n_e)d\sin^2\beta/\lambda\sin\theta$ [53], δ is the phase retardation between the o-ray and e-ray, and β is the angle between the ray in the crystal and the optical axis.

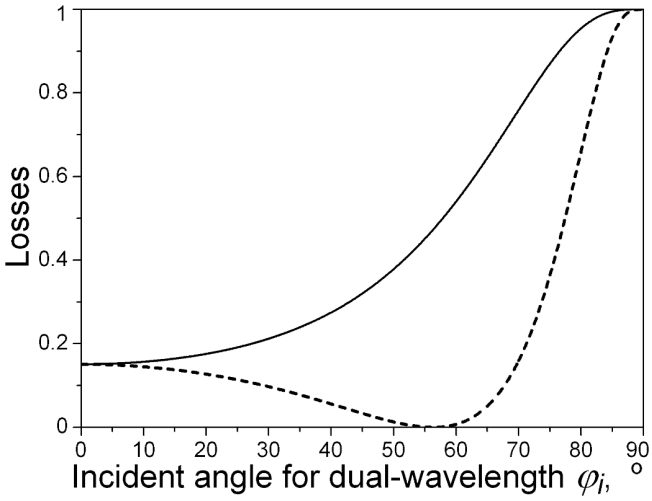

Fig. 3. Dependence of the losses for the π-polarized wave (the solid curve) and σ-polarized wave (the dashed curve) on the incident angle for dual-wavelength operation.

In the matrix elements, the condition for an eigenmode reads

$$M\bar{E} = t\bar{E}, \tag{4}$$

where t is the eigenvalue and $\bar{E}$ is the eigenvector. For the linear laser cavity, the round trip transmittance T of the birefringent filter is expressed as

$$T = |t|^2. \tag{5}$$

The round trip loss of the π and σ-polarized emissions can be written as follows:

$$L_\pi = 1 - T + L_{g\pi}, \tag{6}$$

$$L_\sigma = 1 - T + L_{g\sigma}. \tag{7}$$

In order to successfully suppress lasing at the strong emission line, the threshold power of the weak emission line must be higher than those of the strong emission lines. For a four-level laser, the threshold condition for each transition reads [54]

$$P_{\mathrm{th},i} = \frac{\pi h\nu_p\omega_p^2[\ln(1/R) + L_j]}{2\eta_i f_i\sigma_i\tau[1 - \exp(-2\omega_p^2/\omega_i^2)]}, \tag{8}$$

where R is the reflectivity of output mirror, $\eta_i = \lambda_p/\lambda_i$ is the quantum efficiency, λ_p is pump wavelength, λ_i is lasing wavelength, f_i is the population number in the Stark components of the upper laser level, $h\nu_p$ is the pump photon energy, σ_i is the emission cross section, τ is the fluorescence lifetime, ω_p is the pump beam waist in the active medium, and ω_i the laser beam waist. Here, $j = \pi$, and σ; $i = 1$, 2, 3, 4, 5, 6 represents the nine different laser wavelengths of 519.6, 522.8, 604.5, 607.2 ,719.2, and 721.5 nm, respectively. With Eqs. (1)–(8), the calculated results for the dependence of the threshold and the rotation angle are given in Fig. 4.

The different emission cross sections of the two orthogonal wavelengths result in different gains of the two wavelengths in the cavity. Therefore, the gain and loss of the two wavelengths should be balanced by adjusting the angle of the glass according to the difference of the emission cross section of the two wavelengths of a pair of orthogonal polarizations. The emission cross sections of the 519.6 and 522.8 nm wavelengths are not very different, and we adjust the tilt angle ($20° - 30°$) so that the loss of the two orthogonally polarized wavelengths is also moderate. The emission cross sections of the 604.5 and 607.2 nm wavelengths are quite different, so we adjust the tilt angle ($50° - 60°$) to make the loss of the two orthogonally polarized wavelengths also larger. The difference in emission cross-sections between the 719.2 and 721.5 nm wavelengths is small, so we adjust the tilt angle ($0° - 10°$) so that the loss of the two orthogonally polarized wavelengths is also small.

When the incident angle ϕ_i is adjusted around 20°, the calculated results for the dependence of the threshold at 519.6 and 522.8 nm on the rotation angle of the Lyot filter are given in Fig. 4 a, where one can see that, at the rotation angle $\alpha = 25.7°$, the two wavelengths reach the same threshold.

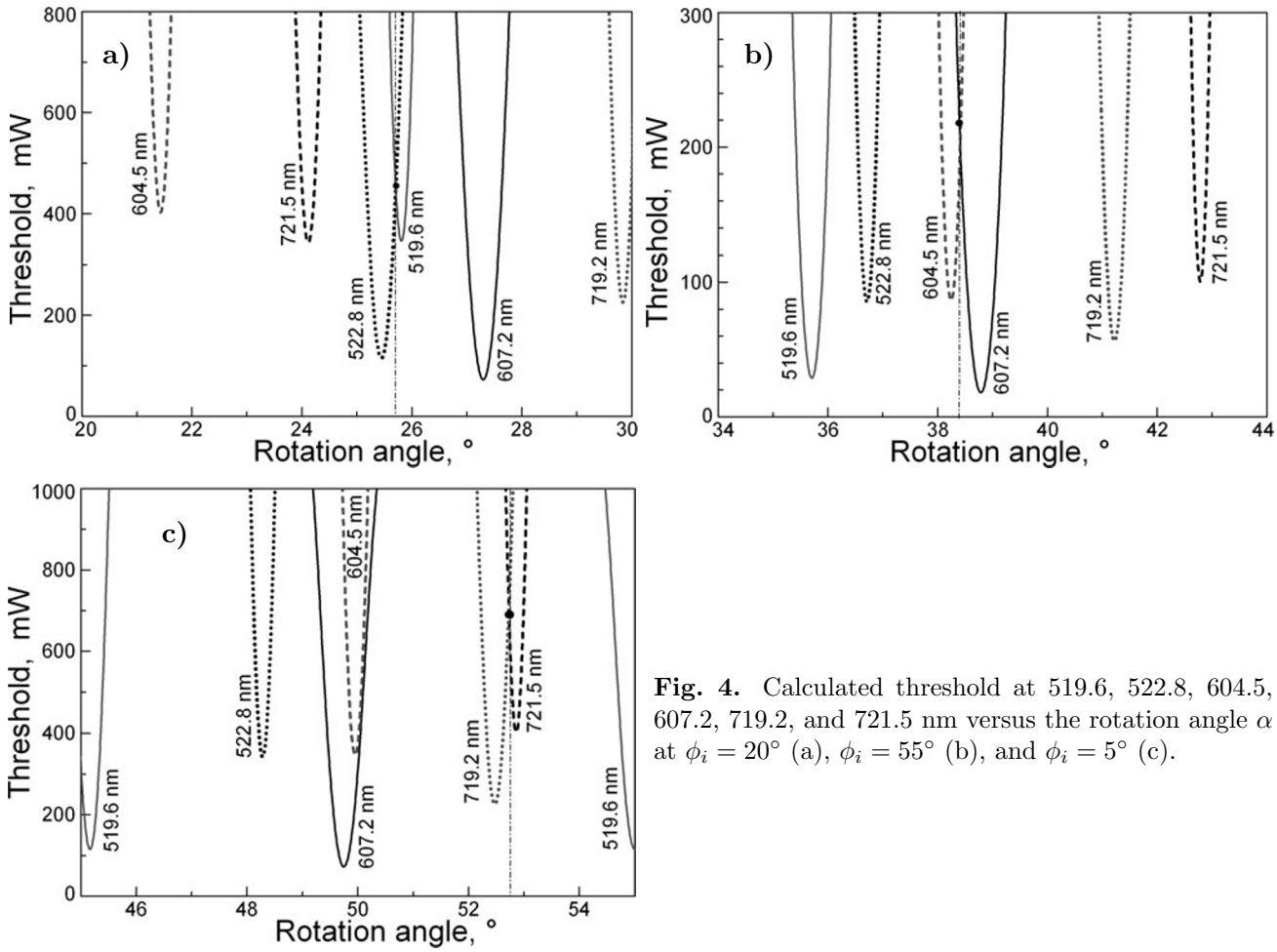

Fig. 4. Calculated threshold at 519.6, 522.8, 604.5, 607.2, 719.2, and 721.5 nm versus the rotation angle α at $\phi_i = 20°$ (a), $\phi_i = 55°$ (b), and $\phi_i = 5°$ (c).

When the incident angle ϕ_i is adjusted around 55°, the calculated results for the dependence of the threshold at 604.5 and 607.2 nm on the rotation angle of the Lyot filter are given in Fig. 4 b, where one can see that, at the rotation angle $\alpha = 38.4°$, the two wavelengths reach the same threshold.

When the incident angle ϕ_i is adjusted around 5°, the calculated results for the dependence of the threshold at 719.2 and 721.5 nm on the rotation angle of the Lyot filter are given in Fig. 4 c, where one can see that, at the rotation angle $\alpha = 52.8°$, the two wavelengths reach the same threshold.

3. Experimental Results

First of all, we adjust the rotation angle α of the Lyot filter to around 26° and the incident angle ϕ_i to around 20°; the same threshold for the dual-wavelength at 519.6 and 522.8 nm is achieved. At a pump power of 4.0 W, the total output powers of 400 mW are obtained. The dual-wavelength operation for different pump powers is shown in the inset of Fig. 5 a. At each pump power level, the Lyot filter should be slightly adjusted to maintain a 1 : 1 spectral intensity ratio of the generated wavelengths. The dual-wavelength laser operation has good stability without power competition between the two wavelengths. It is because the gain and loss are balanced by adjusting the uncoated glass and the Lyot filter. The spectrum of the dual-wavelength laser at a pump power of 4.0 W is shown in the Fig. 5 a. The central

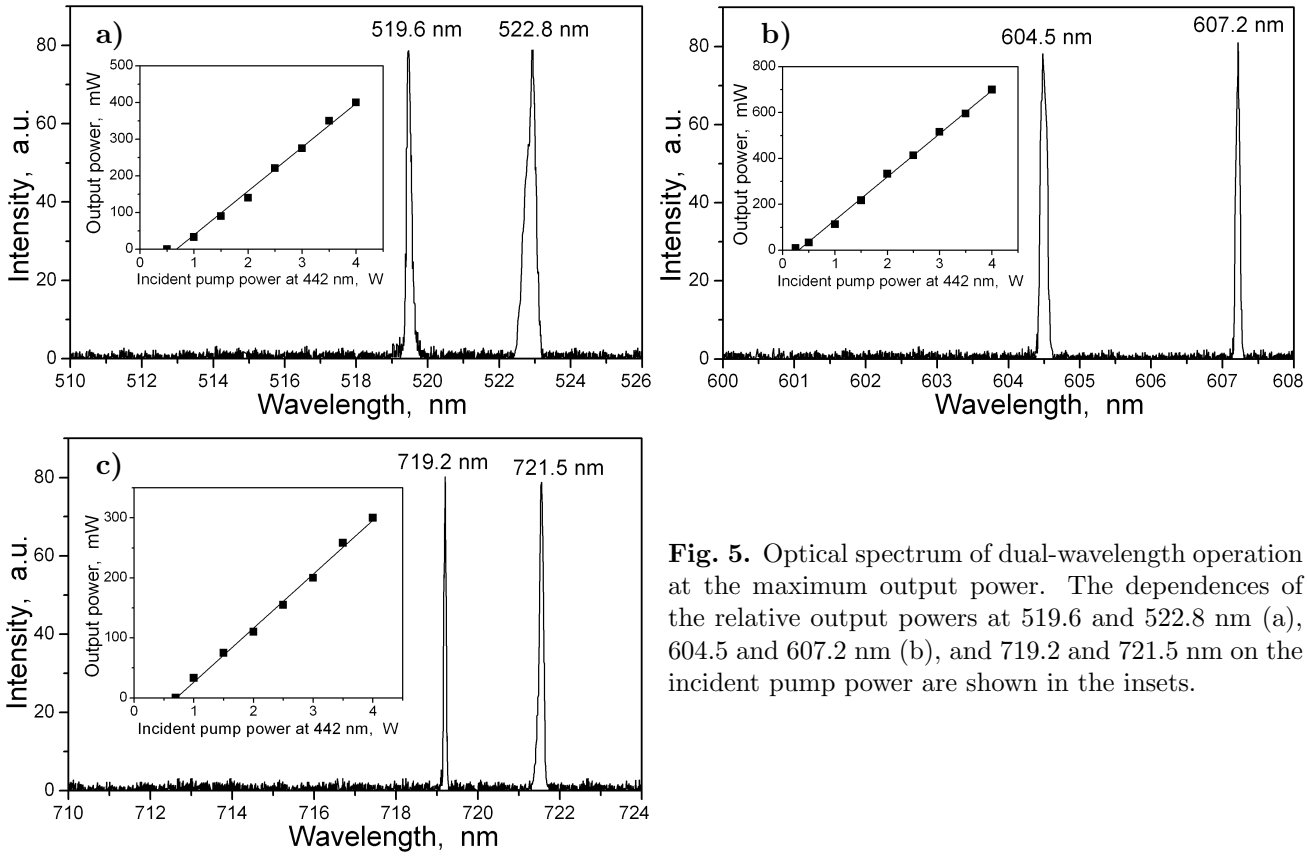

Fig. 5. Optical spectrum of dual-wavelength operation at the maximum output power. The dependences of the relative output powers at 519.6 and 522.8 nm (a), 604.5 and 607.2 nm (b), and 719.2 and 721.5 nm on the incident pump power are shown in the insets.

wavelengths are 519.6 and 522.8 nm, with the optical spectral line widths of 0.20 and 0.23 nm, respectively.

Then, we adjust the rotation angle α of the Lyot filter to around 38° and the incident angle ϕ_i to around 55°; the same threshold for the dual-wavelength at 604.5 and 607.2 nm are achieved. At a pump power of 4.0 W, the total output powers of 700 mW are obtained. The dual-wavelength operation for different pump powers is shown in the inset of Fig. 5 b. The spectrum of the dual-wavelength laser at the pump power of 4.0 W is shown in Fig. 5 b. The central wavelengths are 604.5 and 607.2 nm, with optical spectral line widths of 0.21 and 0.18 nm, respectively. Finally, we adjust the rotation angle α of the Lyot filter to around 53° and the incident angle ϕ_i to around 5°; the same threshold for the dual-wavelength at 719.2 and 721.5 nm is achieved. At a pump power of 4.0 W, total output powers of 300 mW are obtained. The dual-wavelength operation for different pump powers is shown Fig. 5 c (inset). The spectrum of the dual-wavelength laser at a pump power of 4.0 W is shown in Fig. 5 c. The central wavelengths are 719.2 and 721.5 nm, with optical spectral line widths of 0.14 and 0.18 nm, respectively.

4. Summary

In conclusion, we demonstrated a tunable CW orthogonal polarized dual-wavelength laser operation of Pr^{3+}: $LiGdF_4$, using the uncoated glass and the Lyot filter in the laser cavity. We calculated the conditions for balancing the gain and loss of the orthogonal polarization dual-wavelength with the rotation angles of the Lyot filter and the incident angle on the uncoated glass. By adjusting the rotation angle of the Lyot filter and the incident angle on the glass, we obtained for the first time the three pairs of CW orthogonal

polarized dual-wavelength Pr^{3+}:$LiGdF_4$ lasers operating in the visible range. Such multi-wavelength operating regime can lead to discretely tunable multi-wavelength ultraviolet and deep ultraviolet laser sources via nonlinear frequency conversion.

Acknowledgments

This work was supported by the Doctoral Research Initiation Fund Project of the Minzu Normal University of Xingyi under Grant No. 21XYBS19.

References

1. Y. Mao, S. Chang, E. Murdock, et al., *Opt. Lett.*, **36**, 1990 (2011).
2. Y. Li, Z. Du, M. Jia, et al., *Infrared Phys. Technol.*, **133**, 104854 (2023).
3. S. Chang, Y. Mao, and C. Flueraru, *Int. J. Opt.*, **2012**, 565823 (2012).
4. M. Jia, F. Wang, L. Tang, et al., *Opt. Laser Technol.*, **157**, 108634 (2023).
5. M. Jia, L. Tang, K. Teng, et al., *Appl. Surf. Sci.*, **643**, 158641 (2024).
6. S. Buaprathoom, S. Pedley, and S. J. Sweeney, *Proc. SPIE*, **8427**, 84272K (2012).
7. M. Matus, M. Kolesik, J. V. Moloney, et al., *J. Opt. Soc. Am. B*, **21**, 1758 (2004).
8. R. M. Sova, C. S. Kim, and J. U. Kang, *IEEE Photonics Technol. Lett.*, **14**, 287 (2002); 10.1109/68.986788
9. X. Liu, X. Yang, F. Lu, et al., *Opt. Express*, **13**, 142 (2005).
10. L. Guo, R. Lan, H. Liu, et al., *Opt. Express*, **18**, 9098 (2010).
11. B. Yao, Y. Tian, G. Li, et al., *Opt. Express*, **18**, 13574 (2010).
12. H. Yoshioka, S. Nakamura, T. Ogama, et al., *Opt. Express*, **18**, 1479 (2010).
13. H. Maestre, A. J. Torregrosa, C. R. Fernández-Pousa, et al., *Opt. Lett.*, **33**, 1008 (2008).
14. O. J. Zapata-Nava, C. G. Treviño-Palacios, M. D. Iturbe-Castillo, et al., *Opt. Express*, **19**, 3483 (2011).
15. Y. Fujii, and M. Katsuragawa, *Opt. Lett.*, **32**, 3065 (2007).
16. K. Ertel, H. Linné, and J. Bösenberg, *Appl. Opt.*, **44**, 5120 (2005).
17. K. Kawase, M. Mizuno, S. Sohma, et al., *Opt. Lett.*, **24**, 1065 (1999).
18. M. Katsuragawa and T. Onose, *Opt. Lett.*, **30**, 2421 (2005).
19. N. Saito, S. Wada, and H. Tashiro, *J. Opt. Soc. Am. B*, **18**, 1288 (2001).
20. L. Chen, Z. Wang, S. Zhuang, et al., *Opt. Lett.*, **36**, 2554 (2011).
21. G. Shayeganrad and L. Mashhadi, *Appl. Phys. B*, **111**, 189 (2013).
22. E. Herault, F. Balembois, and P. Georges, *Opt. Express*, **13**, 5653 (2005).
23. Y. P. Huang, C. Y. Cho, Y. J. Huang, et al., *Opt. Express*, **20**, 5644 (2012).
24. Y. F. Lü, P. Zhai, J. Xia, et al., *J. Opt. Soc. Am. B*, **29**, 2352 (2012).
25. W. Li, Q. Hao, J. Ding, et al., *J. Opt. A: Pure Appl. Opt.*, **10**, 095307 (2008).
26. S. Zhuang, D. Li, X. Xu, et al., *Appl. Phys. B.*, **107**, 41 (2012).
27. Z. Cong, D. Tang, W. D. Tan, et al., *Opt. Express*, **19**, 3984 (2011).
28. S. D. Liu, L.H. Zheng, J. L. He, et al., *Opt. Express*, **20**, 22448 (2012).
29. M. L. Rico-Soliveres, J. L. Valdes, J. Martinez-Pastor, et al., *Opt. Commun.*, **282**, 1619 (2009).
30. J. Zhang, X. Fu, P. Zhai, et al., *Laser Phys.*, **23**, 115001 (2013).
31. A. Brenier, C. Tu, Z. Zhu, et al., *Appl. Phys. Lett.*, **84**, 16 (2004).
32. X. P. Hu, G. Zhao, Z. Yan, et al., *Opt. Lett.*, **33**, 408 (2008).
33. A. A. Kaminskii, *Quantum Electron.*, **28**, 187 (1998).
34. A. Richter, E. Heumann, E. Osiac, et al., *Opt. Lett.*, **29**, 2638 (2004).
35. Z. Liu, Z. Cai, S. Huang, et al., *J. Opt. Soc. Am. B*, **30**, 302 (2013).
36. S. Luo, B. Xu, S. Cui, et al., *Appl. Opt.*, **54**, 10051 (2015).
37. Y. Cheng, B. Xu, B. Qu, et al., *Appl. Opt.*, **53**, 7898 (2014).

38. T. Gün, P. Metz, and G. Huber, *Opt. Lett.*, **36**, 1002 (2011).
39. B. Xu, F. Starecki, D. Pabœuf, et al., *Opt. Express*, **21**, 5567 (2013).
40. F. Cornacchia, A. Richter, E. Heumann, et al., *Opt. Express*, **15**, 992 (2007).
41. A. Sottile, Z. Zhang, S. Veronesi, et al., *Opt. Mater. Express*, **6**, 1964 (2016).
42. A. Richter, E. Heumann, G. Huber, et al., *Opt. Express*, **15**, 5172 (2007).
43. A. Richter, N. Pavel, E. Heumann, et al., *Opt. Express*, **14**, 3282 (2006).
44. P. Camy, J. L. Doualan, R. Moncorgé, et al., *Opt. Lett.*, **32**, 1462 (2007).
45. A. Sottile and P. W. Metz, *Opt. Lett.*, **40**, 1992 (2015).
46. P. W. Metz, S. Müller, F. Reichert, et al., *Opt. Express*, **21**, 31274 (2013).
47. F. Cornacchia, A. Di Lieto, M. Tonelli, et al., *Opt. Express*, **16**, 15932 (2008).
48. A. Sottile, D. Parisi, and M. Tonelli, *Opt. Express*, **22**, 13784 (2014).
49. J. Xia, Y. Lu, H. Liu, et al., *Opt. Commun.*, **334**, 160 (2015).
50. J. Bai and X. Fu, *Laser Phys.*, **33**, 125001 (2023).
51. J. He, F. Wei, H. Liu, et al., *Laser Phys. Lett.*, **18**, 085003 (2021).
52. M. Born and E. Wolf, *Principles of Optics: Electromagnetic Theory of Propagation, Interference and Diffraction of Light*, 7th (expanded) ed., Cambridge University Press, UK (1999).
53. S. Zhu, *Appl. Opt.*, **29**, 410 (1990).
54. Y. Lü, J. Xia, X. Fu, et al., *J. Opt. Soc. Am. B.*, **31**, 898 (2014).